Available at
http://pvamu.edu/aam
Appl. Appl. Math.
ISSN: 1932-9466

Vol. 11, Issue 1 (June 2016), pp. 251 - 265

Applications and Applied Mathematics:
An International Journal
(AAM)

Enhancement of heat transfer in elastico-viscous fluid due to nanoparticles, where the fluid is impinging obliquely to the stretchable surface: A numerical study

Tariq Javed[1], Abuzar Ghaffari[1] and Tasawar Hayat[2, 3]
[1]Department of Mathematics and Statistic
International Islamic University
Islamabad 44000, Pakistan
[2]Department of Mathematics
Quaid-e-Azam University
Islamabad 44000, Pakistan
[3]Department of Nonlinear Analysis and Applied Mathematics Research Group
Faculty of science
King Abdul Aziz University
Jeddah 21589, Saudi Arabia
abuzar.iiui@gmail.com

Received: June 6, 2015; Accepted: February 9, 2016

Abstract

This article addresses the two-dimensional oblique stagnation point flow of non-Newtonian fluid in the presence of nanoparticles. Constitutive equations of Walter-B fluid are employed in the mathematical development of the relevant problems. Mathematical formulation includes the Brownian motion and thermophoresis effects. The resulting nonlinear system of equations are analyzed through Chebyshev Spectral Newton Iterative Scheme (CSNIS). A comparative study of present results through tabular values has been made with the previous results in a limiting sense and an excellent agreement is noted. It is also found that in near stagnation point region, the heat transfer rate and mass diffusion flux decrease due to increase of thermophoresis effect. However, the heat transfer rate increases and mass diffusion flux decreases as the Brownian motion of the particles increases. The streamlines are drawn to capture the fluid motion.

Keywords: Walter-B nanofluid; oblique stagnation point; Newton Iterative Scheme; Brownian motion; thermophoresis effects.

MSC 2010 No.: 76D10, 82D80, 80A20, 80M22

1. Introduction

There is an increasing interest of recent in the investigation of the dynamics of nanofluids. Such interest, in fact, stems from novel properties of such fluids, which make them potentially useful in heat transfer including pharmaceutical and food processes, hyperthermia, fuel cells, microelectronics, hybrid-powered engines and many others. It is well known that ordinary liquids like water, engine oil and ethylene glycol have poor heat transfer characteristics. On the other hand, most solids especially metals have thermal conductivity one to three times higher than liquids. Thus, nanofluids (fluids that contain nano-sized materials) are considered more adequate to enhance the thermal conductivity of ordinary liquids. Nanoparticles in nano-materials are made of metals (Al, Cu, Ag, Au, Fe), metal carbides (SiC) nonmetals (graphite carbon nanotubes), oxides (Al_2O_3, CuO, TiO_2), nitrides (AIN, SiN) etc. Having such in mind, there is extensive literature available on the topic through different aspects. Few representative studies on the topic may be seen in the references Buongiorno and Hu (2005) to Nadeem and Haq (2015).

A literature survey revealed that much attention in the past has been accorded to the flow of viscous nanofluids. However, in real situations the base fluids in the nano-materials are not viscous. Mention may be made of some viscoelastic nanofluids like ethylene glycol-CuO, ethylene glycol-Al_2O_3, and ethylene glycol-ZnO. Keeping such preference in view, viscoelastic nanofluid is considered in this paper. Many viscoelastic fluids models have been proposed but here constitutive equations of Walter-B fluid (Hayat et al. (2014), Hussain (2011), Beard and Walters (1964)) are employed in the mathematical formulation. Our intention here is to compute the oblique stagnation point flow (Javed et al. (2015) and Javed and Ghaffari (2015)) of viscoelastic nanofluid. To our knowledge, such a problem has not been attempted before. An efficient approach, namely the CSNIS (Majeed et al. (2015)) is implemented for the numerical solution. The graphical results are interpreted with respect to various parameters of interest. A comparison with the previously published results in limiting sense is given. Heat transfer rate and mass diffusion flux are also analyzed.

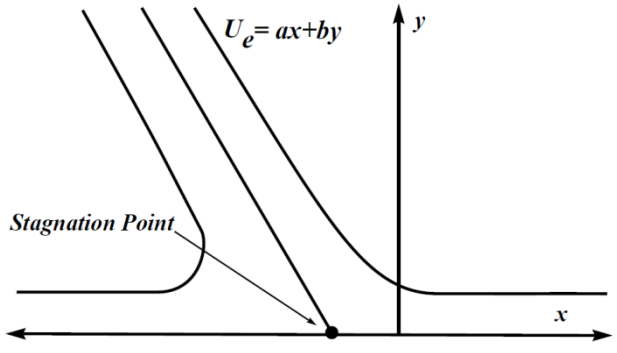

Figure 1: Physical Model

2. Problem formulation

We considered the two-dimensional flow of Walter-B nanofluid. Oblique stagnation point flow is taken. The fluid is impinging obliquely to the stretching sheet at y=0. An incompressible fluid fills the space $y \geq 0$. The governing equations are

$$\frac{\partial \bar{u}}{\partial \bar{x}} + \frac{\partial \bar{v}}{\partial \bar{y}} = 0, \tag{1}$$

$$\bar{u}\frac{\partial \bar{u}}{\partial \bar{x}} + \bar{v}\frac{\partial \bar{u}}{\partial \bar{y}} = -\frac{1}{\rho}\frac{\partial \bar{p}}{\partial \bar{x}} + \nu\left(\frac{\partial^2 \bar{u}}{\partial \bar{x}^2} + \frac{\partial^2 \bar{u}}{\partial \bar{y}^2}\right) + \frac{k_0}{\rho}\left\{\frac{\partial}{\partial \bar{x}}\left[2\bar{u}\frac{\partial^2 \bar{u}}{\partial \bar{x}^2} + 2\bar{v}\frac{\partial^2 \bar{u}}{\partial \bar{x}\partial \bar{y}} + 4\left(\frac{\partial \bar{u}}{\partial \bar{x}}\right)^2 + 2\frac{\partial \bar{v}}{\partial \bar{x}}\left(\frac{\partial \bar{v}}{\partial \bar{x}} + \frac{\partial \bar{u}}{\partial \bar{y}}\right)\right] + \frac{\partial}{\partial \bar{y}}\left[\left(\bar{u}\frac{\partial}{\partial \bar{x}} + \bar{v}\frac{\partial}{\partial \bar{y}}\right)\left(\frac{\partial \bar{v}}{\partial \bar{x}} + \frac{\partial \bar{u}}{\partial \bar{y}}\right) + 2\frac{\partial \bar{u}}{\partial \bar{x}}\frac{\partial \bar{u}}{\partial \bar{y}} + 2\frac{\partial \bar{v}}{\partial \bar{x}}\frac{\partial \bar{v}}{\partial \bar{y}}\right]\right\}, \tag{2}$$

$$\bar{u}\frac{\partial \bar{v}}{\partial \bar{x}} + \bar{v}\frac{\partial \bar{v}}{\partial \bar{y}} = -\frac{1}{\rho}\frac{\partial \bar{p}}{\partial \bar{y}} + \nu\left(\frac{\partial^2 \bar{v}}{\partial \bar{x}^2} + \frac{\partial^2 \bar{v}}{\partial \bar{y}^2}\right) + \frac{k_0}{\rho}\left\{\frac{\partial}{\partial \bar{x}}\left[2\frac{\partial \bar{u}}{\partial \bar{x}}\frac{\partial \bar{u}}{\partial \bar{y}} + 2\frac{\partial \bar{v}}{\partial \bar{x}}\frac{\partial \bar{v}}{\partial \bar{y}} + \left(\bar{u}\frac{\partial}{\partial \bar{x}} + \bar{v}\frac{\partial}{\partial \bar{y}}\right)\left(\frac{\partial \bar{v}}{\partial \bar{x}} + \frac{\partial \bar{u}}{\partial \bar{y}}\right)\right] + \frac{\partial}{\partial \bar{y}}\left[2\frac{\partial \bar{u}}{\partial \bar{y}}\left(\frac{\partial \bar{v}}{\partial \bar{x}} + \frac{\partial \bar{u}}{\partial \bar{y}}\right) + 4\left(\frac{\partial \bar{v}}{\partial \bar{y}}\right)^2 + 2\bar{v}\frac{\partial^2 \bar{v}}{\partial \bar{y}^2} + 2\bar{u}\frac{\partial^2 \bar{v}}{\partial \bar{x}\partial \bar{y}}\right]\right\}, \tag{3}$$

$$\bar{u}\frac{\partial \bar{T}}{\partial \bar{x}} + \bar{v}\frac{\partial \bar{T}}{\partial \bar{y}} = \alpha\left(\frac{\partial^2 \bar{T}}{\partial \bar{x}^2} + \frac{\partial^2 \bar{T}}{\partial \bar{y}^2}\right) + \tau\left[D_B\left(\frac{\partial \bar{C}}{\partial \bar{x}}\frac{\partial \bar{T}}{\partial \bar{x}} + \frac{\partial \bar{C}}{\partial \bar{y}}\frac{\partial \bar{T}}{\partial \bar{y}}\right) + \frac{D_T}{T_\infty}\left[\left(\frac{\partial \bar{T}}{\partial \bar{x}}\right)^2 + \left(\frac{\partial \bar{T}}{\partial \bar{y}}\right)^2\right]\right], \tag{4}$$

$$\bar{u}\frac{\partial \bar{C}}{\partial \bar{x}} + \bar{v}\frac{\partial \bar{C}}{\partial \bar{y}} = D_B\left(\frac{\partial^2 \bar{C}}{\partial \bar{x}^2} + \frac{\partial^2 \bar{C}}{\partial \bar{y}^2}\right) + \frac{D_T}{T_\infty}\left(\frac{\partial^2 \bar{T}}{\partial \bar{x}^2} + \frac{\partial^2 \bar{T}}{\partial \bar{y}^2}\right). \tag{5}$$

In the above equations, $\bar{u}(\bar{x},\bar{y})$ and $\bar{v}(\bar{x},\bar{y})$ are the velocity components in x and y-directions, $\bar{C}(\bar{x},\bar{y})$ and $\bar{T}(\bar{x},\bar{y})$ are the concentration and temperature of the fluid, $\bar{p}(\bar{x},\bar{y})$ is the pressure, α is the thermal diffusivity, ν is the kinematic viscosity, ρ is the density and k_0 is elasticity of fluid. D_T and D_B are the Brownian motion coefficient and Thermophoretic diffusion coefficient, respectively. τ (= $(\rho d)_p/(\rho d)_f$) is the ratio of effective heat capacity of nanoparticles materials to heat capacity of the fluid. It is assumed that the fluid away from the surface is moving with free stream velocity $U_e(\bar{x},\bar{y}) = a\bar{x} + b\bar{y}$. The boundary conditions can be put into the form

$$\begin{aligned} &\bar{y} = 0 \quad : && \bar{u} = c\bar{x},\ \bar{v} = 0, \bar{T} = T_w, \bar{C} = C_w, \\ &\bar{y} \to \infty : && \bar{u} = a\bar{x} + b\bar{y}, \bar{T} = T_\infty, \bar{C} = C_\infty. \end{aligned} \tag{6}$$

in which a, b and c are the positive constant having dimension inverse of time. Here, T_∞ is the ambient temperature of the fluid and T_w is the surface temperature with $T_w > T_\infty$. Setting

$$x=\bar{x}\sqrt{\frac{c}{\nu}},\ y=\bar{y}\sqrt{\frac{c}{\nu}},\ u=\frac{1}{\sqrt{\nu c}}\bar{u},\ v=\frac{1}{\sqrt{\nu c}}\bar{v},\ p=\frac{1}{\rho\nu c}\bar{p},T=\frac{\bar{T}-T_\infty}{T_w-T_\infty},C=\frac{\bar{C}-C_\infty}{C_w-C_\infty},\quad (7)$$

we obtain the resulting problems as follows:

$$\frac{\partial u}{\partial x}+\frac{\partial v}{\partial y}=0, \quad (8)$$

$$u\frac{\partial u}{\partial x}+v\frac{\partial u}{\partial y}=-\frac{\partial p}{\partial x}+\left(\frac{\partial^2 u}{\partial x^2}+\frac{\partial^2 u}{\partial y^2}\right)+We\left\{\frac{\partial}{\partial x}\left[2u\frac{\partial^2 u}{\partial x^2}+2v\frac{\partial^2 u}{\partial x\partial y}+4\left(\frac{\partial u}{\partial x}\right)^2+2\frac{\partial v}{\partial x}\left(\frac{\partial v}{\partial x}+\frac{\partial u}{\partial y}\right)\right]+\frac{\partial}{\partial y}\left[\left(u\frac{\partial}{\partial x}+v\frac{\partial}{\partial y}\right)\left(\frac{\partial v}{\partial x}+\frac{\partial u}{\partial y}\right)+2\frac{\partial u}{\partial x}\frac{\partial u}{\partial y}+2\frac{\partial v}{\partial x}\frac{\partial v}{\partial y}\right]\right\}, \quad (9)$$

$$u\frac{\partial v}{\partial x}+v\frac{\partial v}{\partial y}=-\frac{\partial p}{\partial y}+\left(\frac{\partial^2 v}{\partial x^2}+\frac{\partial^2 v}{\partial y^2}\right)+We\left\{\frac{\partial}{\partial x}\left[2\frac{\partial u}{\partial x}\frac{\partial u}{\partial y}+2\frac{\partial v}{\partial x}\frac{\partial v}{\partial y}+\left(u\frac{\partial}{\partial x}+v\frac{\partial}{\partial y}\right)\left(\frac{\partial v}{\partial x}+\frac{\partial u}{\partial y}\right)\right]+\frac{\partial}{\partial y}\left[2\frac{\partial u}{\partial y}\left(\frac{\partial v}{\partial x}+\frac{\partial u}{\partial y}\right)+4\left(\frac{\partial v}{\partial y}\right)^2+2v\frac{\partial^2 v}{\partial x^2}+2u\frac{\partial^2 v}{\partial x\partial y}\right]\right\}, \quad (10)$$

$$\Pr\left[u\frac{\partial T}{\partial x}+v\frac{\partial T}{\partial y}\right]=\left(\frac{\partial^2 T}{\partial x^2}+\frac{\partial^2 T}{\partial y^2}\right)+\Pr\left[N_b\left(\frac{\partial C}{\partial x}\frac{\partial T}{\partial x}+\frac{\partial C}{\partial y}\frac{\partial T}{\partial y}\right)+N_t\left[\left(\frac{\partial T}{\partial x}\right)^2+\left(\frac{\partial T}{\partial y}\right)^2\right]\right], \quad (11)$$

$$Sc\left[u\frac{\partial C}{\partial x}+v\frac{\partial C}{\partial y}\right]=\left(\frac{\partial^2 C}{\partial x^2}+\frac{\partial^2 C}{\partial y^2}\right)+\frac{N_t}{N_b}\left(\frac{\partial^2 T}{\partial x^2}+\frac{\partial^2 T}{\partial y^2}\right), \quad (12)$$

$$\begin{aligned} &y=0 \quad : && u=x,\ v=0,T=1,C=1,\\ &y\to\infty: && u=\frac{a}{c}x+\frac{b}{c}y,T=0,C=0, \end{aligned} \quad (13)$$

where $We=k_0c/\rho\nu$ is the Weissenberg number, $\Pr=\nu/\alpha$ is the Prandtl number, $Sc=\nu/D_B$ is the Schmidt number $N_t=D_T\,\tau(T_w-T_\infty)/T_\infty\nu$ is the thermophoresis parameter and $N_b=D_B\tau(C_w-C_\infty)/\nu$ is the Brownian motion parameter. Incompressibility condition is satisfied by considering stream function ψ by

$$u=\frac{\partial\psi}{\partial y},\ v=-\frac{\partial\psi}{\partial x}. \quad (14)$$

Equations (9) – (14), through eliminating pressure, yield

$$\frac{\partial\left(\psi,\nabla^2\psi\right)}{\partial\left(x,y\right)}+We\frac{\partial\left(\psi,\nabla^4\psi\right)}{\partial\left(x,y\right)}+\nabla^4\psi=0, \tag{15}$$

$$\Pr\left[\frac{\partial\psi}{\partial y}\frac{\partial T}{\partial x}-\frac{\partial\psi}{\partial x}\frac{\partial T}{\partial y}\right]=\left(\frac{\partial^2 T}{\partial x^2}+\frac{\partial^2 T}{\partial y^2}\right)+\Pr\left[N_b\left(\frac{\partial C}{\partial x}\frac{\partial T}{\partial x}+\frac{\partial C}{\partial y}\frac{\partial T}{\partial y}\right)+N_t\left[\left(\frac{\partial T}{\partial x}\right)^2+\left(\frac{\partial T}{\partial y}\right)^2\right]\right], \tag{16}$$

$$Sc\left[\frac{\partial\psi}{\partial y}\frac{\partial C}{\partial x}-\frac{\partial\psi}{\partial x}\frac{\partial C}{\partial y}\right]=\left(\frac{\partial^2 C}{\partial x^2}+\frac{\partial^2 C}{\partial y^2}\right)+\frac{N_t}{N_b}\left(\frac{\partial^2 T}{\partial x^2}+\frac{\partial^2 T}{\partial y^2}\right), \tag{17}$$

$$\begin{aligned} y=0 \quad &: \qquad \frac{\partial\psi}{\partial y}=x,\ \psi=0, T=1, C=1, \\ y\to\infty &: \qquad \psi=\frac{a}{c}xy+\frac{\gamma}{2}y^2, T=0_\infty, C=0, \end{aligned} \tag{18}$$

with $\gamma = b/c$ which represents shear in the stream. We write the solution of Equations (15) – (18) as follows:

$$\psi=xf(y)+g(y),\quad T=\theta(y),\quad C=\phi(y), \tag{19}$$

where the functions $f(y)$ and $g(y)$ are assumed normal and oblique component of the flows. Putting Equation (19) into Equations (15) – (18), and then comparing the coefficients of x^0 and x^1, one arrives at

$$f^{iv}+ff'''-f'f''+We\left(ff^{v}-f'f^{iv}\right)=0, \tag{20}$$

$$g^{iv}+fg'''-g'f''+We\left(fg^{v}-g'f^{iv}\right)=0, \tag{21}$$

$$\theta''+\Pr\left[f\theta'+N_b\phi'\theta'+N_t\left(\theta'\right)^2\right]=0, \tag{22}$$

$$\phi''+Sc\,f\phi'+\left(\frac{N_t}{N_b}\right)\theta''=0, \tag{23}$$

$$\begin{aligned} y=0 \quad &: \qquad f(y)=0,\ f'(y)=1,\ g(y)=g'(y)=0,\ \theta(y)=1, \phi(y)=1, \\ y\to\infty &: \qquad f'(y)=a/c,\ g'(y)=\gamma y,\ \theta(y)=0,\ \phi(y)=0. \end{aligned} \tag{24}$$

Here, prime signifies the differentiation with respect to y. Integration of Equations (20) and (21) and gives

$$f'''+ff''-\left(f'\right)^2+We\left(ff^{iv}-2f'f'''+\left(f''\right)^2\right)+\frac{a^2}{c^2}=0, \tag{25}$$

$$g'''+fg''-g'f'+We\left(fg^{iv}-f'g'''+g''f''-f'''g'\right)-A\gamma=0, \tag{26}$$

where the constant A accounts for boundary layer displacement. It arises since when $y\to\infty$,

$f(y)$ behaves as $f(y)=(a/c)y+A$. For simplicity, introducing a new variable, $g'(y)=\gamma h(y)$ then Equation (26) with boundary conditions can be expressed in the forms

$$h''+fh'-f'h+We\left(fh'''-f'h''+h'f''-f'''h\right)=A, \tag{27}$$

$$h(0)=0 \quad h'(\infty)=1. \tag{28}$$

The resulting system is

$$f'''+ff''-(f')^2+We\left(ff^{iv}-2f'f'''+(f'')^2\right)+\frac{a^2}{c^2}=0, \tag{29}$$

$$h''+fh'-f'h+We\left(fh'''-f'h''+h'f''-f'''h\right)=A, \tag{30}$$

$$\theta''+\Pr\left[f\theta'+N_b\phi'\theta'+N_t(\theta')^2\right]=0, \tag{31}$$

$$\phi''+Sc\,f\phi'+\left(\frac{N_t}{N_b}\right)\theta''=0, \tag{32}$$

$$\begin{aligned} y=0 \quad &: \quad f(y)=0,\ f'(y)=1,\ h(y)=0,\ \theta(y)=1,\phi(y)=1,\\ y\to\infty &: \quad f'(y)=a/c,\ h'(y)=1,\theta(y)=0,\phi(y)=0. \end{aligned} \tag{33}$$

Dimensionless components of velocity are

$$u=\frac{\partial\psi}{\partial y}=xf'(y)+g'(y) \tag{34}$$

and

$$v=-\frac{\partial\psi}{\partial x}=-f(y). \tag{35}$$

The skin friction coefficient C_f, the local Nusselt number Nu_x and the local Sherwood number Sh_x, are

$$C_f=\frac{\tau_w}{\rho u_w^2};\quad Nu_x=\frac{xq_w}{k(T_w-T_\infty)};\quad Sh_x=\frac{xq_m}{D_B(C_w-C_\infty)}, \tag{36}$$

where τ_w is shear stress at the wall and q_w and q_m indicating local heat flux and local mass diffusion flux are

$$\tau_w=\mu\left(\bar{u}_{\bar{y}}+\bar{v}_{\bar{x}}\right)-2k_0\left(\begin{array}{c} -\bar{u}_{\bar{y}}\bar{v}_{\bar{y}}-\bar{u}_{\bar{x}}\bar{v}_{\bar{x}}-\frac{1}{2}\bar{v}_{\bar{y}}\left(\bar{u}_{\bar{y}}+\bar{v}_{\bar{x}}\right)-\frac{1}{2}\bar{u}_{\bar{x}}\left(\bar{u}_{\bar{y}}+\bar{v}_{\bar{x}}\right)+\\ \frac{1}{2}\bar{v}\left(\bar{u}_{\bar{y}\bar{y}}+\bar{v}_{\bar{x}\bar{y}}\right)+\frac{1}{2}\bar{u}\left(\bar{u}_{\bar{x}\bar{y}}+\bar{v}_{\bar{x}\bar{x}}\right) \end{array}\right)\Bigg|_{\bar{y}=0}, \tag{37}$$

$$q_w=-k\left(\frac{\partial\bar{T}}{\partial\bar{y}}\right)\Bigg|_{\bar{y}=0},\quad q_m=-D_B\left(\frac{\partial\bar{C}}{\partial\bar{y}}\right)\Bigg|_{\bar{y}=0}.$$

The skin friction coefficient C_f, the local Nusselt number Nu_x and the local Sherwood number Sh_x, after using Equations (7), (14) and (19) are

$$\begin{aligned} &\mathrm{Re}_x C_f = x(1-3We) f''(0) + (1-2We)\gamma h'(0), \\ &\mathrm{Re}_x^{-1/2} Nu_x = -\theta'(0), \ \mathrm{Re}_x^{-1/2} Sh_x = -\phi'(0), \end{aligned} \tag{38}$$

where $\mathrm{Re}_x = u_w^2 / c\nu$.

3. Numerical method

For the solution of Equations (29) – (33), Chebyshev Spectral Newton Iterative Scheme (CSNIS) is used. Here, we convert the system of nonlinear differential equation into a linear form by using Newton iterative scheme as a first step. For (i+1)*th* iterates we write

$$f_{i+1} = f_i + \delta f_i, \tag{39}$$

for all dependent variables. Using Equation (39) in Equation (29), one has

$$c_{0,i}\delta f_i^{iv} + c_{1,i}\delta f_i''' + c_{2,i}\delta f_i'' + c_{3,i}\delta f_i' + c_{4,i}\delta f_i = R_i, \tag{40}$$

subject to boundary conditions

$$\delta f_i(0) = -f_i(0), \ \delta f_i'(0) = a/c - f_i'(0), \quad \delta f_i'(\infty) = 1 - f_i'(\infty). \tag{41}$$

The coefficients $c_{j,i}$ (j=0, 1, 2, 3, 4) and R_i are

$$\begin{aligned} c_{0,i} = We\, f_i,\ c_{1,i} = 1 - 2We\, f_i',\ c_{2,i} = f_i - 2We\, f_i'', \\ c_{3,i} = -2f_i' - 2We\, f_i''',\ c_{4,i} = f_i'' + We\, f_i^{iv}, \\ R_i = -We\left(f_i f_i^{iv} - 2 f_i' f_i''' + \left(f_i''\right)^2 \right) - f_i''' - f_i f_i'' + \left(f_i'\right)^2 - a^2/c^2. \end{aligned} \tag{42}$$

Equation (40) is now linear and is solved using the Chebyshev Spectral Collocation Method (Motsa et al. (2014), Motsa (2013)). For this purpose, the physical domain [0, ∞] is truncated to finite domain [0, L], where L is chosen sufficiently large to achieve the accuracy. The reduced domain is transformed to [-1, 1] by using transformation $\xi = 2\eta/L - 1$. Nodes from –1 to 1 are defined as $\xi_j = \cos(\pi j/N)$, j=0, 1, 2, … N, which are known as Gauss-Lobatto collocation points. In the present problem we choose the value of N = 120. The Chebyshev Spectral Collocation Method is based on differentiation matrix $\boldsymbol{D}$, which can be computed in different ways. Here, we used $\boldsymbol{D}$ as suggested by Trefethen (2000). For i=0, Equations (39) and (40) become

$$\begin{aligned} f_1 = f_0 + \delta f_0, \\ c_{0,0}\delta f_0^{iv} + c_{1,0}\delta f_0''' + c_{2,0}\delta f_0'' + c_{3,0}\delta f_0' + c_{4,0}\delta f_0 = R_0, \end{aligned} \tag{43}$$

where f_0 is used as an initial guess and we found δf_0 for first iteration. Similarly for i =1, Equation (39) and (40) become

$$f_2 = f_1 + \delta f_1,$$
$$c_{0,1}\delta f_1^{iv} + c_{1,1}\delta f_1''' + c_{2,1}\delta f_1'' + c_{3,1}\delta f_1' + c_{4,1}\delta f_1 = R_1, \tag{44}$$

where $f_1 = f_0 + \delta f_0$ is known function and we found δf_1 for second iteration from Equation (44). We continue this procedure until $f_{i+1} - f_i \approx 0$. Thus, the Equation (29) subject to the boundary condition (33) has been solved and the solution f is obtained. Now Equation (30) becomes linear and it is solved by using the Chebyshev Spectral Collocation Method. It should be noted that the energy equation defined in Equation (31) is still non-linear which can be solved by following similar steps as explained for Equation (30). Hence, the system through Equations (30) and (32) becomes linear which is solved by using the Chebyshev Spectral Collocation Method directly without employing the Newton iterative scheme. Matlab (R2010a) is utilized to develop the algorithm for this purpose.

4. Results and discussion

The non-linear differential Equations (29) – (32) with boundary conditions (33) are solved numerically for the different values of the pertinent parameters. Chebyshev Spectral Newton Iterative Scheme (CSNIS) is implemented for the solution. A comparative study is also performed with limiting existing studies. In Tables 1 and 2, the comparison of obtained results with Hussain et al. (2011), Ishak et al. (2007) and Mahapatra and Gupta (2000) is made. These limiting results are in very good agreement with the results proposed by Hussain et al. (2011) and Ishak et al. (2007). Table 1 is evidence that $f''(0)$ acts as an increasing function of the ratio of straining to stretching velocities *a/c* and decreasing function of Weissenberg number *We*. Table 2 shows with the increase in *a/c* and *Pr*, the absolute value of $\theta'(0)$ increases; this is in good agreement with the results proposed by Mahapatra and Gupta (2000). In Table 3, the values of local Nusselt ($\mathrm{Re}_x^{-1/2} Nu_x$) and the local Sherwood ($\mathrm{Re}_x^{-1/2} Sh_x$) numbers are shown for some important values of different parameters.

Table 1. Comparison of $f''(0)$ for the various values of *a/c* and *We*.

We	*a/c*	Present Results	Hussain et al. (2011)	Ishak et al. (2007)
0	0.01	−0.9981	–	−0.9980
	0.1	−0.9694	−0.9693	−0.9694
	0.2	−0.9181	–	−0.9181
	0.5	−0.6673	−0.6672	−0.6673
	1.1	0.1643	0.1642	–
	1.2	0.3377	0.3377	–
	2.0	2.0175	–	2.0175
	3.0	4.7293	–	4.7294
	10.0	36.2574	–	36.2603
0.1	0.1	−1.0273	−1.0271	–
	0.5	−0.7300	−0.7299	–
	1.1	0.1918	0.19177	–
	1.2	0.3993	0.3992	–
0.2	0.1	−1.0956	−1.0955	–
	0.5	−0.8102	−0.8101	–
	1.1	0.2393	0.2392	–
	1.2	0.5140	0.5139	–
0.3	0.1	−1.1778	−1.1777	–
	0.5	−0.9142	−0.9141	–
	1.1	0.3520	0.35198	–
	1.2	0.9103	0.8499	–

Table 2. Comparison of $\theta'(0)$ for various values of *a/c* and *Pr* when thermophoresis effects and Brownian motion of nanoparticles are absent

a/c	Present Results	Mahapatra and Gupta (2000)	Present Results	Mahapatra and Gupta (2000)
	Pr = 1		*Pr = 1.5*	
0.1	−0.6022	−0.603	−0.7768	−0.777
0.2	−0.6245	−0.625	−0.7971	−0.797
0.5	−0.6924	−0.692	−0.8648	−0.863
1.0	−0.7979	−0.796	−0.9772	−0.974
2.0	−0.9787	−0.974	−1.1781	−1.171
3.0	−1.1321	−1.124	−1.3519	−1.341

Table 3. Numerical values of physical quantities for different values of *We*, *a/c*, *Nt*, *Nb*, *Sc* and *Pr*.

We	*a/c*	*Nt*	*Nb*	*Sc*	*Pr*	$-Re_x^{-1/2} Nu_x$	$-Re_x^{-1/2} Sh$
0	0.1	0.1	0.1	1	1	0.5552	0.2575
0	0.1	0.1	0.2	1	7	1.2561	0.1482
0.1	0.1	0.1	0.5	1	10	0.6868	0.5161
0.1	0.2	0.5	0.1	5	1	0.4605	0.8795
0.2	0.2	0.5	0.2	5	7	0.3395	1.7338
0.3	0.2	0.5	0.5	5	10	0.0391	1.7854

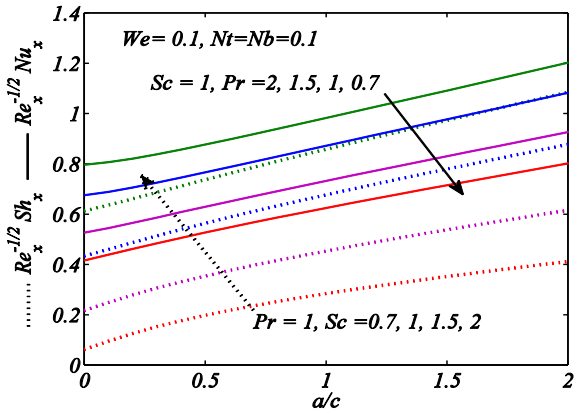

Figure 2. Variation of heat flux and mass diffusion flux against *a/c* for different values of *Sc* and *Pr*

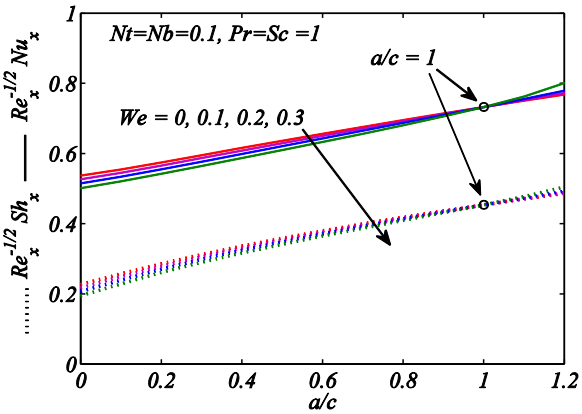

Figure 3. Variation of heat flux and mass diffusion flux against *a/c* for different values of *We*

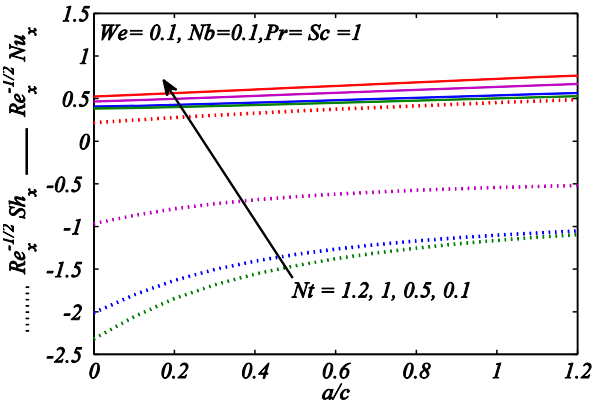

Figure 4. Variation of heat flux and mass diffusion flux against *a/c* for different values of N_t.

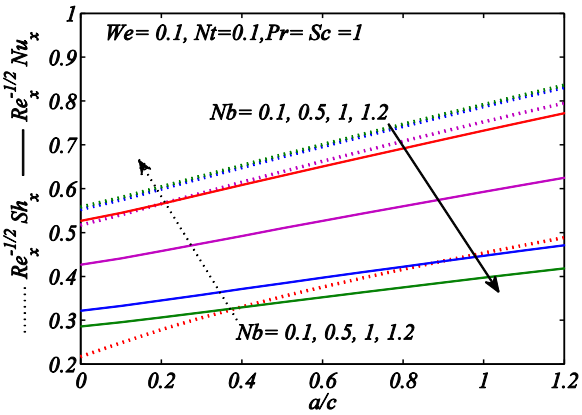

Figure 5. Variation of heat flux and mass diffusion flux against *a/c* for different values of N_b

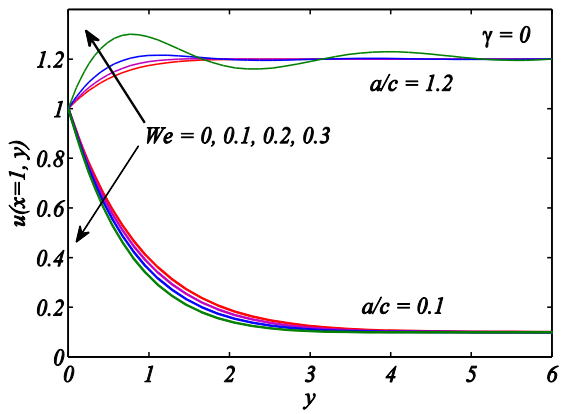

Figure 6. Orthogonal velocity profile for different values of *We* when *a/c* is equal to 0.1 and 1.2

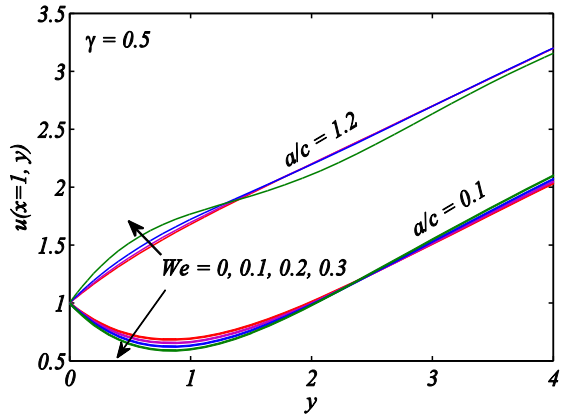

Figure 7. Non-orthogonal velocity profile for different values of *We* when *a/c* is equal to 0.1 and 1.2

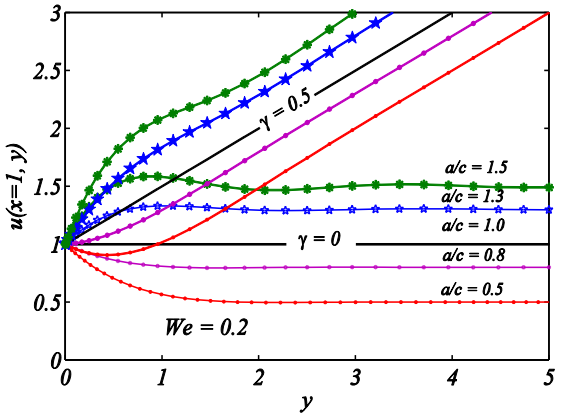

Figure 8. Orthogonal and non-orthogonal velocity profile for different values of *a/c* when *We* =0.2

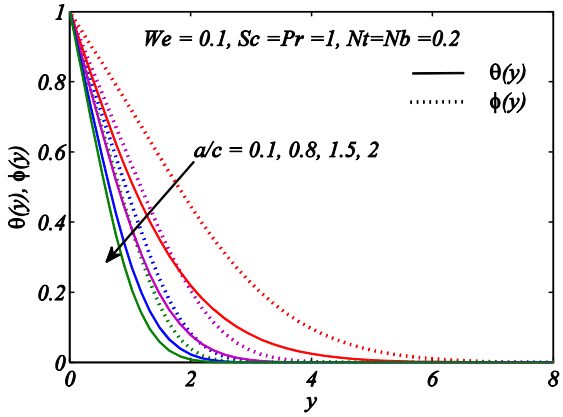

Figure 9. Variations of $\theta(y)$ and $\phi(y)$ for different values of *a/c*

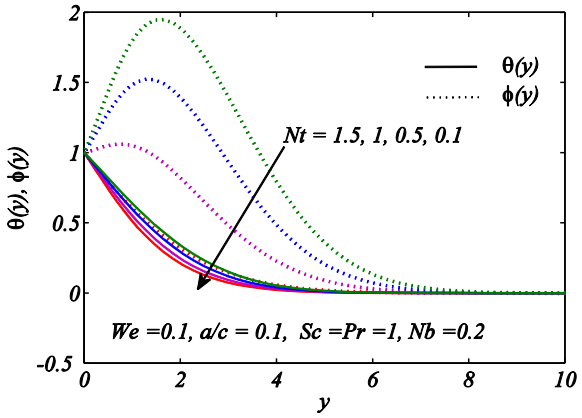

Figure 10. Variations of $\theta(y)$ and $\phi(y)$ for different values of N_t

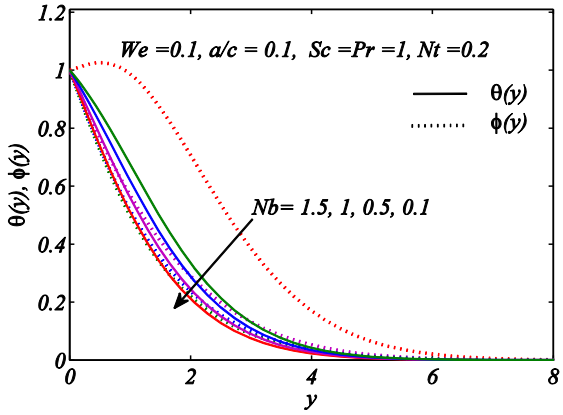

Figure 11. Variations of $\theta(y)$ and $\phi(y)$ for different values of N_b

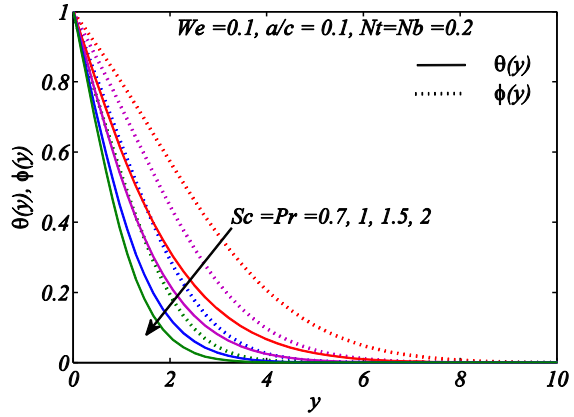

Figure 12. Variations of $\theta(y)$ and $\phi(y)$ for different values of *Sc*

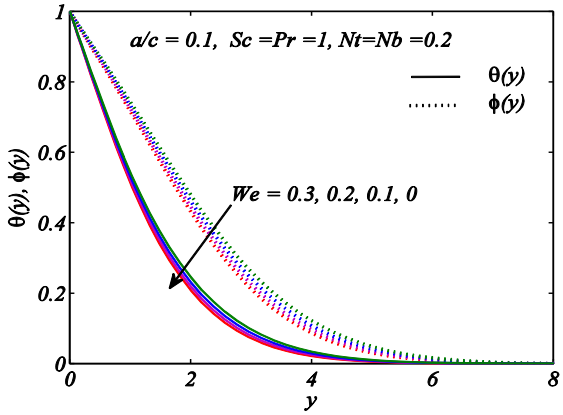

Figure 13. Variations of $\theta(y)$ and $\phi(y)$ for different values of *We*

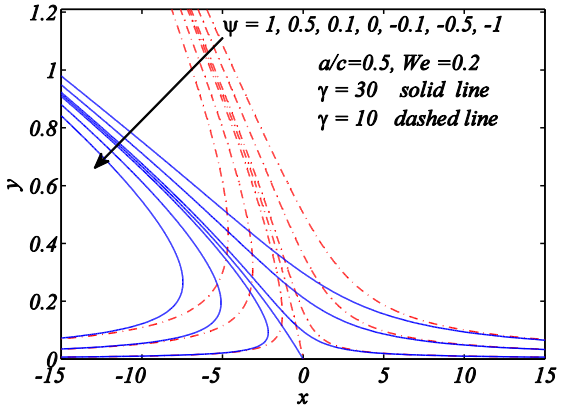

Figure 14. Stream lines for different values of γ

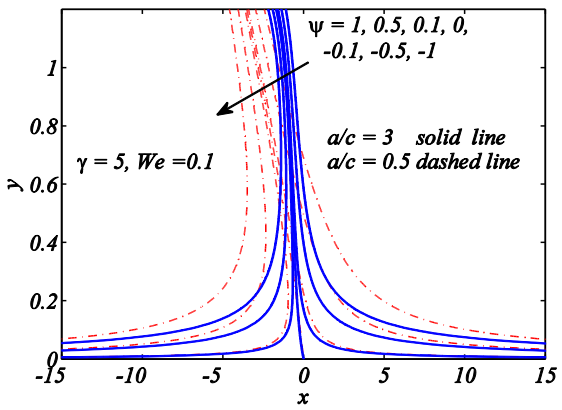

Figure 15. Stream lines for different values of *a/c*

Figure 2 represents the local Nusselt number and local Sherwood number against the ratio parameter *a/c* for the various values of Prandtl number (*Pr*) and Schmidt number (Sc), when *We*=0.1, N_t= N_b=0.1 and *Pr*=1(for reduced Nusselt), *Sc*=1(for Sherwood number). It is observed that both the local Nuesselt and local Sherwood numbers are increasing functions of Prandtl and Schmidt numbers, respectively. In addition, the heat transfer rate and mass diffusion flux are enhanced for larger *a/c*. In Figure 3 the variations of local Nusselt and local Sherwood numbers are plotted against the velocities ratio parameter *a/c*. Here, different values of *We* are taken when N_t = N_b = 0.1 and *Pr* = *Sc* = 1. It is noted that larger *We* leads to a decrease in both local Nusselt and local Sherwood numbers. Inverted boundary layer structure in flow occurs when stretching velocity becomes higher than the free stream velocity i.e., *a/c*<1. As expected, no boundary layer exits for *a/c*=1. Figure 3 shows that for *a/c*=1 the local Nusselt and local Sherwood numbers remain unchanged against Weissenberg number *We*. For *a/c*>1 (when free steam velocity is higher than the stretching velocity), the local Nusselt and local Sherwood numbers are increasing functions of *We*.

In Figures 4 and 5, the effect of thermophoresis (thermodiffusion) N_t and Brownian motion N_b parameters on local Nusselt number $\mathrm{Re}_x^{-1/2}Nu_x$ and local Sherwood number $\mathrm{Re}_x^{-1/2}Sh_x$ are discussed. In Figure 4, it is noted that the heat transfer rate and mass diffusion start decreasing near the stagnation point when N_t increases. In Figure 5, the local Nusselt number decreases by increasing the Brownian motion of the particle but the mass diffusion flux increases through an increase in Brownian motion parameter. From Figures 4 and 5 it is also noted that with the increase of free stream velocity (i.e., *ax*) both quantities (i.e., local Nusselt and Sherwood numbers) increase but, on the other hand, as the stretching velocity increases, these quantities start decreasing. In Figures 6 and 7, both orthogonal and non-orthogonal velocity profiles are drawn against *y* for different values of viscoelastic parameter (*We*), respectively. In these figures both cases of boundary layer (*a/c* > 1) and inverted boundary layer (*a/c* < 1) are discussed. When *a/c* < 1, the boundary layer thickness decreases by increasing viscoelastic parameter. For *a/c* > 1, the velocity of fluid increases near the wall for larger *We* but away from the wall it starts fluctuating in the main stream for non-zero values of *We*.

In Figure 8, orthogonal (γ=0) and non-orthogonal (γ=0.5) velocity profiles are drawn against *y*

for the various values of velocities ratio parameter *a/c*. In case of non-orthogonal flow, the velocity of the fluid is much greater than orthogonal flow for all values of $a/c > 0$. It is also noted that the velocity of the fluid increases for larger *a/c* in both cases of orthogonal and non-orthogonal stagnation point flow. The velocity of fluid becomes constant for $a/c = 1$ (when both stretching and straining velocities become equal). The variation of temperature and concentration profiles are analyzed in the Figures 9-13. In Figure 9, it is observed that both the temperature and concentration of the fluid decreases when the free stream velocity rapidly increases more than the stretching velocity. Figures 10 and 11 indicate that the temperature and concentration are increasing functions of thermophoresis (thermodiffusion) N_t and random motion of the particles (Brownian motion) N_b. Figure 12 shows that with the increase of *Pr* and *Sc*, the heat transfer rate and diffusion flux are enhanced. The thermal and concentration boundary layer thickness decrease. The viscoelastic effect on temperature and concentration profiles is shown in Figure 13. It is found that both the temperature and concentration profiles are increasing functions of *We*.

Figures 14 and 15 show that the effect of γ and the velocity ratio parameters *a/c* on the stream lines. In Figure 14 the streamlines become closer to the plate and the boundary layer thickness reduces when γ enhances. The streamlines are drawn for the values of ψ=1, 0.5, 0.1, 0, -0.1, -0.5, -1 and the fixed values of $a/c = 0.5$, $We = 0.2$. At $\psi = 0$, a straight line is formed which is known as dividing streamline. In Figure 15, by increasing the velocity ratio parameter *a/c*, the streamlines look like those for the orthogonal stagnation point flow. The streamlines are drawn for $a/c = 0.5$ (dashed lines) and $a/c = 3$ (solid lines) and clearly the solid lines are less oblique than the dashed lines.

5. Concluding remarks

The study on oblique stagnation point flow of non-Newtonian nanofluid over a stretching surface is presented in the present study. The solution of the problem is obtained by Chebyshev Spectral Newton Iteration Scheme (CSNIS). The method is presented in detail and results are compared with previous studies through tables. The results are found in good agreement. It is also observed that CSNIS is efficient, less time consuming, stable and with rapid convergence. It is found near the stagnation point that for larger thermophoresis effect, the heat transfer rate and mass diffusion flux decrease; however the temperature and concentration of the fluid increase. With the increase in Brownian motion of the particles, the heat transfer rate increases and mass diffusion flux decreases. The present study also reveals that for $a/c < 1$, the heat transfer rate as well as shear wood number decrease with the increase in the value of Wiesenberger number and an opposite behavior has been observed for $a/c > 1$.

REFERENCES

Abbasi, F.M., Hayat, T. and Alsaedi, A. (2015). Peristaltic transport of magneto-nanoparticles submerged in water: Model for drug delivery system, Phasica E, vol. 68, pp. 123-132.

Bachok, N., Ishak, A. and Pop, I. (2010). Boundary-layer flow of nanofluids over a moving surface in a flowing fluid, Int J Thermal Sci. vol. 49, pp. 1663–1668.

Beard, D. W. and Walters, K. (1964). Elastico-viscous boundary-layer flows. I. Two-dimensional flow near a stagnation point, Proc. Cambridge Philos. Soc. vol. 60, pp. 667–674.

Buongiorno, J. and Hu, L.W (2005). Nanofluid Coolants for Advanced Nuclear Power Plants, Paper No. 5705, Proceedings of ICAPP , Seoul, pp. 15–19.

Choi, S.U.S. (1995). Enhancing thermal conductivity of fluids with nanoparticles, in: Developments and Application of Non-Newtonian Flows, FED-vol. 231/MD vol. 66, pp. 99–105.

Farooq, U., Hayat, T., Alsaedi, A. and Liao S. (2014). Heat and mass transfer of two-layer flows of third-grade nano-fluids in a vertical channel, Appl. Math. Computation, vol. 242, pp. 528-540.

Hamad, M.A.A. and Ferdows, M. (2012). Similarity solution of boundary layer stagnation-point flow towards a heated porous stretching sheet saturated with a nanofluid with heat absorption/generation and suction/blowing: a Lie group analysis. Commun Nonlinear Sci Numer Simulat, vol. 17, pp. 132–40.

Hassani, M., Tabar, M.M., Nemati, H., Domairry, G. and Noori, F. (2011). An analytical solution for boundary layer flow of a nanofluid past a stretching sheet, Int J Therm Sci, vol. 50, pp. 2256–63.

Hayat, T., Asad, S., Mustafa, M. and Alsulami, H.H. (2014). Heat transfer analysis in the flow of Walters' B fluid with a convective boundary condition, Chin. Phys. B. vol. 23(8) No. 084701.

Hussain, I., Labropulu, F. and Pop, I. (2011). Two-dimensional oblique stagnation-point flow towards a stretching surface in a viscoelastic fluid, Cent. Eur. J. Phys. Vol. 9(1) pp. 176-182.

Ishak, A., Nazar R., N. Arifin, M. and Pop, I. (2007). Mixed convection of the stagnation-point flow towards a stretching vertical permeable sheet, Malaysian J. Mathematical Sciences, Vol. 1(2), pp.217 - 226.

Javed, T., Ghaffari, A. and Ahmad, H. (2015). Numerical Study of Unsteady Oblique Stagnation Point Flow Over an Oscillating Flat Plate, Canadian Journal of Physics, vol. 93(10), pp. 1138-1143.

Javed, T. and Ghaffari, A. (2015). Numerical Study of Non-Newtonian Maxwell Fluid in the Majeed, A., Javed. T., Ghaffari, A. and Rashidi, M.M., Analysis of Heat Transfer due to

Kameswaran, P.K., Shaw, S., Sibanda, P. and Murthy P.V.S.N. (2013). Homogeneous–Heterogeneous reactions in a nanofluid flow due to a porous stretching sheet, Int. J. Heat Mass Transfer, vol. 57, pp. 465-472.

Kumar, K.Ch. and Bandari, S. (2014). Melting heat transfer in boundary layer stagnation-point flow of a nanofluid towards a stretching/ shrinking sheet, Can. J. of Phys. vol. 92 pp. 1703-1708.

Kuznetsov, A.V. and Nield, D.A. (2011). Double-diffusive natural convective boundary-layer flow of a nanofluid past a vertical plate, Int J Thermal Sci, vol. 50, pp. 712–717.

Kuznetsov, A.V. and Nield, D.A. (2010). Natural convective boundary-layer flow of a nanofluid past a vertical plate, Int. J. Therm. Sci. vol. 49, pp. 243–247.

Mahapatra, T.R. and Gupta, A.S. (2000). Heat transfer in stagnation point flow towards stretching sheet, Heat and Mass Transfer, vol. 38, pp. 517-521.

Makinde, O.D and Aziz, A. (2011). Boundary layer flow of a nanofluid past a stretching sheet with a convective boundary condition. Int J Thermal Sci. vol. 50, pp.1326–1332.

Makinde, O.D. (2012). Analysis of Sakiadis flow of nanofluids with viscous dissipation and Newtonian heating. Appl Math Mech. Vol. 33(12), pp. 1545–1554.

Motsa, S. S., Dlamini, P. G., and Khumalo, M. (2014). Spectral relaxation method and spectral quasi-linearization method for solving unsteady boundary layer flow problems, Advances in Mathematical Physics, Article ID 341964.

Motsa, S. S. (2013). A new Spectral local Linearization method for nonlinear boundary layer flow problems, Journal of Applied Mathematics, Article ID 423628.

Mustafa, I., Javed, T. and Majeed A., Magnetohydrodynamic (MHD) mixed convection stagnation point flow of a nanofluid over a vertical plate with viscous dissipation, Canadian Journal of Physics, 2015, 93(11): 1365-1374.

Mustafa T. (2014). Nanofluid flow and heat transfer due to a rotating disk, Computer and fluids, vol. 94, pp. 139-146.

Nadeem, S. and Haq, RU. (2015). MHD boundary layer flow of a nanofluid past a porous shrinking sheet with thermal radiation, J Aerosp Eng, vol. 28(2), No. 04014061.

Rahman, M.M., Rosca, A.V. and Pop I. (2014). Boundary layer flow of a nanofluid past a permeable exponentially shrinking/stretching surface with second order slip using Buongiorno's model, Int. J. Heat Mass Transfer, vol. 77 pp. 1133-1143.

Rana, P. and Bhargava, R. (2012). Flow and heat transfer of a nanofluid over a nonlinearly stretching sheet: a numerical study. Commun Nonlinear Sci Numer Simulat, vol. 17, pp. 212–26.

Rashidi, M.M., Vishnu, G. N., Abdul Hakeem., A.K. and Ganga B. (2014). Buoyancy effect on MHD flow of nanofluid over a stretching sheet in the presence of thermal radiation, J. Molecular Liquids, vol. 198, pp. 234-238.

Region of Oblique Stagnation Point Flow over a Stretching Sheet. Journal of Mechanics, available on CJO2015. doi:10.1017/jmech.2015.94.

Sebdani, S.M., Mahmoodi, M, Hashemi, S. (2012). Effect of nanofluid variable properties on mixed convection in a square cavity. Int J Thermal Sci. vol. 52, pp. 112–126.

Sheikholeslami, M., Hatami, M. and Domairry G. (2015). Numerical simulation of two phase unsteady nanofluid flow and heat transfer between parallel plates in presence of time dependent magnetic field, J. Taiwan Institute Chem. Eng. vol. 46 pp. 43-50.

Sheikholeslami, M., Gorji-Bandpy, M., Ganji, D.D., Rana, P. and Soleimani, S. (2014). Magnetohydrodynamic free convection of Al2O3–water nanofluid considering Thermophoresis and Brownian motion effects, Computer and fluids, vol. 94, pp. 147-160.

Stretching Cylinder with Partial Slip and Prescribed Heat Flux: A Chebyshev Spectral Newton Iterative Scheme, Alexandria Engineering Journal, (2015).

Trefethen, L.N., (2000). Spectral Methods in MATLAB, Society for Industrial and Applied Mathematics, SIAM, Philadelphia, *Pa, USA.*